On the Enhancement of Generalized Integrator-based Adaptive Filter Dynamic Tuning Range

Hafiz Ahmed, *Member, IEEE*, and Mohamed Benbouzid, *Fellow, IEEE*

***Abstract*—Many phase locked-loop (PLL) or frequency locked-loop (FLL) use quadrature signals (directly or indirectly) as the input variables. Generalized integrator (GI) is a popular quadrature signal generator (QSG) available in the literature. GI is also widely used in various industrial applications. In addition to being a QSG, GI also works as kind of band-pass filter. However, due to structural limitation, the dynamic tuning range is limited for the standard GI. The limitation arises from using only one gain in the direct-phase estimation dynamics while quadrature phase estimation dynamics doesn't use direct feedback of the filter estimation error. Some attempts have already been made to overcome this limitation by adding direct feedback of the filter estimation error to quadrature phase dynamics as well. However, we have demonstrated in this paper that this kind of implementation has some frequency domain limitations. In this paper, we propose a novel GI type adaptive filter using coordinate transformation. The resulting structure maintains the same kind of filtering property of the standard GI at the transformed coordinates level while at the same time enhances the dynamic tuning range of standard GI. Details of the proposed technique, stability analysis and discussion on gain tuning are provided in this paper. Finally, comparative experimental results are provided with respect to GI-FLL to show the dynamic performance improvement. Experimental results demonstrate the suitability of the proposed technique.**

***Index Terms*—Frequency Estimation, Phase Estimation, Frequency-Locked Loop, GI-FLL, Adaptive Filter, Generalized Integrator.**

I. Introduction

PHASE, frequency, symmetrical components etc. are important parameters of electric grid voltage signal. Many power and industrial electronics application require the precise knowledge of these parameters for various, monitoring and control functions e.g. wide-area monitoring [1]–[3], grid-connected converters (GCC) [4], [5], active power filter [6], symmetrical components extraction [7], grid ancillary services [8] to name a few. This has led to an increasing research effort on estimating these parameters of grid voltage signal.

Many techniques are currently available in the literature. They cover an wide array of methods and exploit various characteristics of the grid voltage signal. Some of the techniques are signal transformation-based techniques (including various variants of Fourier transforms) [9], [10], least-square regression [11], maximum-likelihood techniques [12], [13], filter with dynamic gains [14], function approximation-based technique [15], state-space methods [16], filter with fixed gains [17]–[23], adaptive notch filter [24], derivative estimation-based technique [25], phase-locked loop (PLL) [26]–[34], self-tuning filter [6], etc. to name a few.

Many of the above mentioned techniques, use quadrature signals as the fundamental building block. As the grid parameters are generally unknown with known nominal values, generating the quadrature signal is not straight forward. In this regard quadrature signal generator (QSG) are very useful. Generalized integrator-based approach [18], [19], [35] is one of the most popular QSG technique available in the literature. GI essentially uses the model of well known linear harmonic oscillator. GI can be used in conjunction with both FLL and PLL. In this paper, we limit our attention to GI-FLL. The results presented on the improvement of GI are equally applicable to GI-PLL.

In GI-FLL, GI part generates the quadrature signals while FLL part uses the generated signals for unknown frequency estimation purpose. GI part uses only one fixed gain in the in-phase dynamics part while no gains are used in the quadrature phase estimation part. The closed-loop poles of the GI part are: $-0.5k_s\omega \pm \omega\sqrt{k_s^2-4}$, where k_s is the feedback gain and ω is the grid frequency (*cf.* Sec. II-A for details). Since GI generates oscillatory signal, complex conjugate poles are desirable for the GI. However, the closed-loop poles remain complex conjugates as long as the filter gain is selected as $k_s < 2$. In this case, the real part of the closed-loop poles can not be set further than $-\omega$ in the complex plane. It is well known from the literature [36] that real part of the pole determines the convergence speed. This limits the dynamic tuning range of the GI part in term of complex conjugate pole placement. One potential solution is to use additional gain in the quadrature phase estimation part. Although this enables arbitrary complex-conjugate pole placement but comes at the cost of reduction in filtering property. This can be evident from the transfer functions given in Sec-II-B. In the standard GI case, the direct and quadrature phase maintains a perfect 90° phase difference for all frequency range. However, this is not true for the GI that uses two gains (*cf.* Sec. II-B for more details). As such this limits the application of GI with two gains in practice.

To overcome the above mentioned filtering and dynamic gain limitations of GI (with one and two gains), in this paper we propose another technique. In the proposed technique,

H. Ahmed is with the School of Mechanical, Aerospace and Automotive Engineering, Coventry University, Coventry CV1 5FB, United Kingdom (E-mail: hafiz.h.ahmed@ieee.org).
M. Benbouzid is with the University of Brest, UMR CNRS 6027 IRDL, 29238 Brest, France and Shanghai Maritime University, 201306 Shanghai, China (E-mail: mohamed.benbouzid@univ-brest.fr).

state-variables of the standard GI are transformed first. This allows to enhance the dynamic tuning range while at the same time maintaining the filtering properties of the standard GI in the transformed coordinates. The resulting solution enhances the dynamic tuning range of the standard GI by approximately 2.5 times with some additional computational cost. This modification of the standard GI is the main contribution of this paper.

The rest of the paper is organized as follows: Sec. II describes the proposed technique, stability analysis, tuning and extension to three-phase case. Experimental results are given in Sec. III while Sec. IV concludes this paper.

II. Proposed Approach

A. Standard GI-FLL

Single-phase grid voltage signal is modeled as a sine wave and given by:

$$\nu = A\sin(\underbrace{\omega t + \phi}_{\theta}) \tag{1}$$

where A, ω, ϕ, θ denotes the amplitude, angular frequency, phase and instantaneous phase respectively. GI-FLL estimates the parameter of grid voltage signal (1) by generating quadrature signals. For that purpose, let us consider the direct-phase signal as $v_d = v$ and the quadrature-phase signal as $v_q = -A\cos(\theta)$. Then the following algorithm describes the process of estimating v_d and v_q using only the measurement of v_d and given by [37, Chapter 4]:

$$\dot{\eta}_s = \hat{A}_s\eta_s + L_s e_s \tag{2a}$$
$$\hat{\nu}_s = C_s\eta_s \tag{2b}$$
$$\dot{\hat{z}} = -\beta_s\hat{\omega}\eta_{qs}e_s \tag{2c}$$
$$\dot{\hat{z}} = \frac{-\beta_s\hat{\omega}\eta_{qs}e_s}{\eta_{ds}^2+\eta_{qs}^2} \tag{2d}$$

where, $\hat{}$ represents estimated value, $\eta_s = \begin{bmatrix} \eta_{qs} & \eta_{ds} \end{bmatrix}^T$ is the state vector, the matrices are given by,

$$\hat{A}_s = \begin{bmatrix} 0 & \hat{\omega} \\ -\hat{\omega} & 0 \end{bmatrix},$$
$$C_s = \begin{bmatrix} 0 & 1 \end{bmatrix},$$
$$L_s = \begin{bmatrix} 0 & k_s\hat{\omega} \end{bmatrix}^T,$$

$e_s = \nu - \hat{\nu}_s$ is the output estimation error, $\eta_{ds} = \hat{v}_d$, $\eta_{qs} = \hat{v}_q$, k_s, β_s are tuning gains,, $\omega = \omega_n + z$ with $\omega_n = 100\pi$ being the nominal frequency. In this work, we assume that the unknown frequency, ω as an unknown constant. Through experimental results in Sec. III-B, it is shown that despite this assumption, the proposed technique is able to track time varying grid frequency. Graphical representation of GI-FLL is given in Fig. 1. In eq. (2), quadrature signals are estimated by the GI part i.e. eq. (2a) and (2b) while the unknown grid frequency is estimated by the FLL part given by eq. (2c). Eq. (2d) is the FLL with gain normalization which is very useful in the context of adding low voltage ride through capability to the control scheme of grid-connected inverters. Poles of the GI part are the eigenvalues of the matrix $\hat{A}_s - L_sC_s$ and are calculated as: $-0.5k_s\hat{\omega} \pm \hat{\omega}\sqrt{k_s^2-4}$. Since GI part generate oscillatory signals, complex conjugate poles are generally preferred. However, for any $k_s \geq 2$, system poles are no longer complex conjugate. For any $0 < k_s < 2$, the real part of the system poles always have a value greater than $-\hat{\omega}$. As a result, dynamic tuning range is limited. This motivates us to further develop standard GI-FLL without sacrificing much the excellent filtering property. To demonstrate the filtering property of standard GI-FLL, the transfer functions are given below:

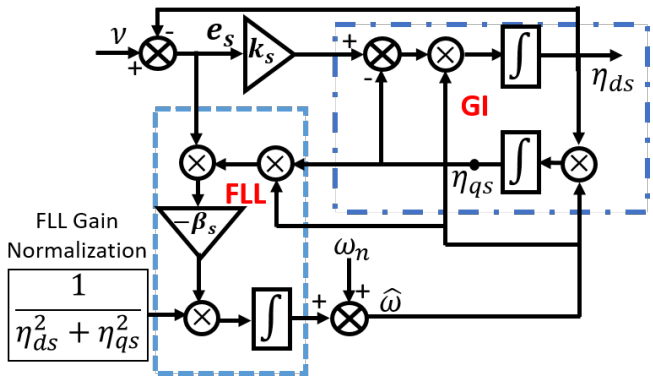

Figure 1. Block diagram of GI-FLL [37].

$$D_s(s) = \frac{\eta_{ds}}{v}(s) = \frac{k_s\hat{\omega}s}{s^2+k_s\hat{\omega}s+\hat{\omega}^2} \tag{3a}$$
$$Q_s(s) = \frac{\eta_{qs}}{v}(s) = \frac{k_s\hat{\omega}^2}{s^2+k_s\hat{\omega}s+\hat{\omega}^2} \tag{3b}$$
$$E_s(s) = \frac{e_s}{v}(s) = \frac{s^2+\hat{\omega}^2}{s^2+k_s\hat{\omega}s+\hat{\omega}^2} \tag{3c}$$

From eq. (3a) it is clear that GI is a band-pass type filter where the bandwidth is uniquely determined by k_s. This frequency selective property makes GI as an ideal candidate to generate quadrature signals even in the distorted conditions. Moreover, the two transfer functions (i.e. eq. (3a) and (3b)) maintain a perfect 90° phase difference in any frequency range.

B. GI-type observer (GIO)

To increase the dynamic tuning range of GI-FLL, an observer-based framework can be considered similar to the ideas presented in [20], [38]. In this framework, in addition to eq. (2b), the error feedback is also injected to eq. (2a). In the observer framework, the implementation of GIO-FLL is given below:

$$\dot{\eta}_o = \hat{A}_o\eta_o + L_o e_o \tag{4a}$$
$$\hat{\nu}_o = C_o\eta_o \tag{4b}$$
$$\dot{z} = -\beta_o\hat{\omega}\eta_{qo}e_o \tag{4c}$$
$$\dot{z} = \frac{-\beta_o\hat{\omega}\eta_{qo}e_o}{\eta_{do}^2+\eta_{qo}^2} \tag{4d}$$

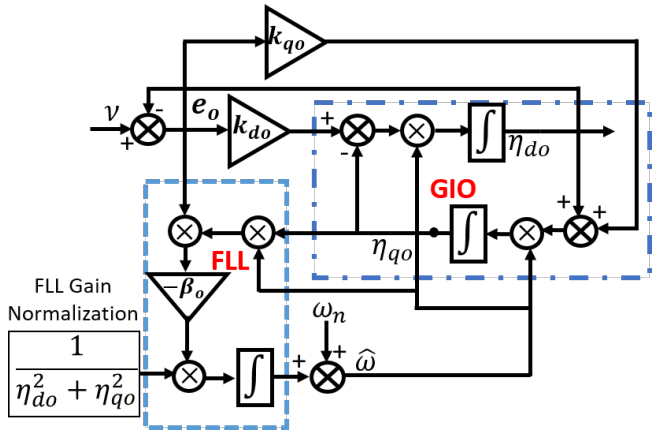

Figure 2. Block diagram of GIO-FLL.

where $L_0 = \begin{bmatrix} k_{qo}\hat{\omega} & k_{do}\hat{\omega} \end{bmatrix}^T$ and all the other variables and matrices retain the same meaning as explained in Sec. II-A. Block diagram of GIO-FLL is given in Fig. 2. In this case, the system poles of the GIO are the eigenvalues of the matrix $\hat{A}_o - L_o C_o$ and are calculated as: $-0.5k_{do}\hat{\omega} \pm 0.5\hat{\omega}\sqrt{k_{do}^2 + 4k_{qo} - 4}$. If we set $k_{qo} = -k_{do}^2/4$, then the poles are: $-0.5k_{do}\hat{\omega} \pm i\hat{\omega}$. This means, for any $k_{do} > 4$, the system poles will always have negative real part with complex conjugate imaginary part. As such wide range of tuning is possible as opposed to standard GI. The tuning of the observer gain can be performed using pole placement. Wide tuning range comes at the cost of reduction in filtering property. To demonstrate the filtering property of the GIO-FLL, the transfer functions are given below:

$$D_o(s) = \frac{\eta_{d0}}{v}(s) = \frac{k_{do}\hat{\omega}s - k_{qo}\hat{\omega}^2}{s^2 + k_{do}\hat{\omega}s + \hat{\omega}^2(1 - k_{qo})} \tag{5a}$$

$$Q_o(s) = \frac{\eta_{qo}}{v}(s) = \frac{k_{qo}\hat{\omega}s + k_{do}\hat{\omega}^2}{s^2 + k_{do}\hat{\omega}s + \hat{\omega}^2(1 - k_{qo})} \tag{5b}$$

$$E_o(s) = \frac{e_o}{v}(s) = \frac{s^2 + \hat{\omega}^2}{s^2 + k_{do}\hat{\omega}s + \hat{\omega}^2(1 - k_{qo})} \tag{5c}$$

From the transfer functions (5), it is evident that unlike standard GI, the observer-based implementation doesn't maintain the perfect 90° phase difference between the direct-phase and the quadrature-phase signal i.e. eq. (5a) and (5b) for all frequency range (*cf.* Fig. 3). Moreover, as shown in Fig. 4, FLL input variables don't have perfect in-phase relationship for $\omega < \omega_r$ and out of phase relationship for $\omega > \omega_r$ with ω_r being the resonance frequency. This may lead to oscillation in the estimated frequency. As such, the application in practice can be limited although a wide range of dynamic tuning is possible in this type of implementation. The observer uses the error feedback gain in both direct and quadrature-axes dynamics. The objective of the observer is to make sure that the estimation error converges to zero asymptotically, while the objective of the filter is to minimize the effect of noise and disturbances. As such, the design philosophy of observer and filter are not the same. This contributes to the change in QSG characteristics in the observer-based implementation of standard GI-FLL.

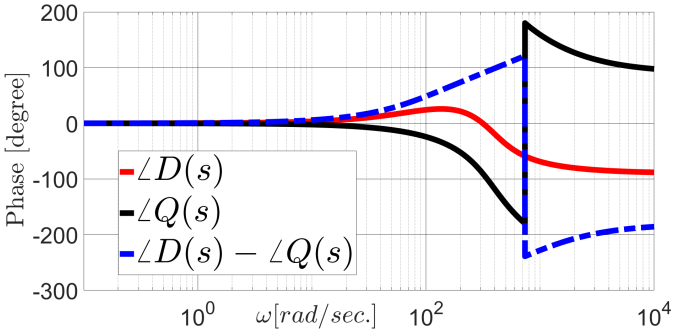

Figure 3. Bode phase plot of $D_o(s)$ and $Q_o(s)$ with $k_{do} = \sqrt{2}$ and $k_{qo} = -0.5$.

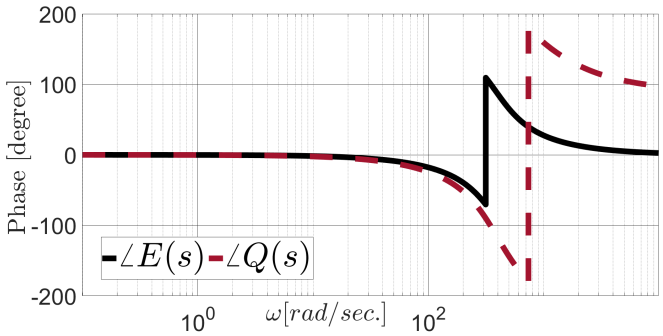

Figure 4. Bode phase plot of FLL input variables for the GIO-FLL.

C. GI type adaptive filter design

Sec. II-A demonstrated the dynamic tuning limitation of standard GI-FLL while Sec. II-B showed the filtering limitation of an alternative solution. This Section will discuss the development of the proposed filter that presents a compromise between the filter and observer-based implementation. To this end, let us consider two new state variables given as:

$$\eta_1 = \frac{1}{\omega_n^2 + \hat{\omega}^2}\left(\frac{\omega}{\omega_n}\eta_{qf} + \eta_{df}\right) \tag{6a}$$

$$\eta_2 = \frac{1}{\omega_n^2 + \omega^2}\left(-\omega\eta_{qf} + \frac{\omega^2}{\omega_n}\eta_{df}\right) \tag{6b}$$

where f stands for the filter and the variables retain the same meaning as described earlier i.e. $\eta_{df} = A\sin(\theta)$, and $\eta_{qf} = -A\cos(\theta)$. In the new state variables, GI-type frequency adaptive filter is given by:

$$\dot{\hat{\eta}} = \hat{A}_f\hat{\eta} + L_f e_f \tag{7a}$$

$$\hat{\nu}_f = C_f\hat{\eta} \tag{7b}$$

$$\dot{\hat{z}} = -\beta_f\hat{\eta}_1\hat{\omega}e_f \tag{7c}$$

$$\dot{\hat{z}} = \frac{-\beta_f\hat{\eta}_1\hat{\omega}e_f}{\hat{\eta}_1^2 + (\hat{\eta}_2/\hat{\omega})^2} \tag{7d}$$

where $\hat{\eta} = \begin{bmatrix} \hat{\eta}_1 & \hat{\eta}_2 \end{bmatrix}^T$ is the state vector, the matrices are given by:

$$\hat{A}_f = \begin{bmatrix} 0 & 1 \\ -\hat{\omega}^2 & 0 \end{bmatrix},$$
$$C_f = \begin{bmatrix} \omega_n^2 & \omega_n \end{bmatrix},$$
$$L_f = \begin{bmatrix} 0 & k_f \end{bmatrix},$$

$e_f = \nu - \hat{\nu}_f$ is the output estimation error of the filter, and $k_f > 0$ is the filter gain. Similar to standard GI, proposed GI-type filter (GTF) uses only one gain. To demonstrate the filtering property of the proposed GTF-FLL, let us consider the transfer function given below:

$$D_f(s) = \frac{\hat{\eta}_2}{v}(s) = \frac{k_f s}{s^2 + k_f\hat{\omega}s + \hat{\omega}^2(1+k_f)} \tag{8a}$$
$$Q_f(s) = \frac{\hat{\eta}_1}{v}(s) = \frac{k_f}{s^2 + k_f\hat{\omega}s + \hat{\omega}^2(1+k_f)} \tag{8b}$$
$$E_f(s) = \frac{e_f}{v}(s) = \frac{s^2 + \hat{\omega}^2}{s^2 + k_f\hat{\omega}s + \hat{\omega}^2(1+k_f)} \tag{8c}$$

Similar to standard GI, proposed GTF is also a band-pass filter and the filter bandwidth is uniquely determined by the filter gain k_f. Moreover, the two transfer functions (i.e. eq. (8a) and (8b)) maintain a perfect 90° phase difference in any frequency range. This demonstrated the equivalence of the proposed technique with standard GI. Next, let us consider the system poles of GTF. The system poles of the GTF part are the eigenvalues of the matrix $\hat{A}_f - L_f C_f$ and are calculated as: $-0.5k_f\hat{\omega} \pm 0.5\hat{\omega}\sqrt{k_f^2 - 4k_f - 4}$. For any value of $0 < k_f \leq 4.82$, the system poles always have negative real parts with complex-conjugate imaginary parts. By considering $k_f = 0.1$, the pole locations can be found as $-0.05\hat{\omega} \pm 1.0476i$ while for $k_f = 4.82$, the pole locations are $-2.41\hat{\omega} \pm 0.1091i$.

Moreover, the real part of the system poles always have a value greater than or equal to $-2.41\hat{\omega}$ inside the selected k_f range as opposed to $-\hat{\omega}$ for the standard GI. As a result, it can be considered that the proposed GTF enhances the dynamic tuning range of GI.

From $\hat{\eta}_1$ and $\hat{\eta}_2$, $\hat{\eta}_{qf}$and $\hat{\eta}_{df}$ can be obtained using the following formula:

$$\hat{\eta}_{qf} = \omega_n\hat{\omega}\hat{\eta}_1 - (\omega_n^2/\hat{\omega})\hat{\eta}_2 \tag{9a}$$
$$\hat{\eta}_{df} = \omega_n^2\hat{\eta}_1 + \omega_n\hat{\eta}_2 \tag{9b}$$

From the estimated direct and quadrature-phase signals, the instantaneous phase of the grid voltage signal can be estimated as:

$$\hat{\theta} = \arctan2(\eta_{df}, -\eta_{qf}) \tag{10}$$

FLL Analysis: The proposed GTF is frequency adaptive and requires the estimated frequency $\hat{\omega}$. FLL is very suitable for this purpose. Following the ideas of standard FLL as given in Sec. II-A, the FLL considered in this work is given in eq. (7c) where β_f is the FLL tuning parameter. Bode diagram phase plot of the FLL input variables is given in Fig. 5. From Fig. 5, it can be seen that the input variables are in phase when $\omega < \omega_r$ and out of phase when $\omega > \omega_r$. As such, the input variables are very suitable to detect any change in the frequency. The behavior of the proposed FLL is similar to standard FLL where same relationship can be observed between the FLL input variables.

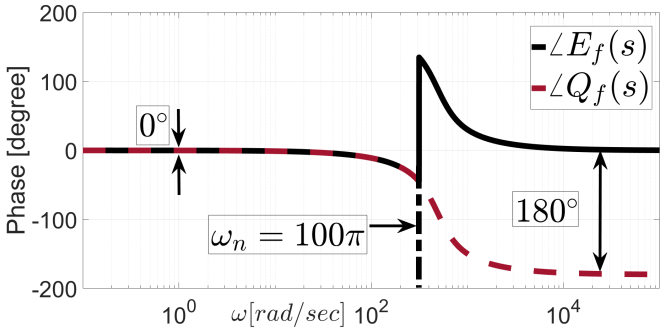

Figure 5. Bode diagram phase plot of the FLL input variables with $k_f = \sqrt{2}$.

It is to be noted here that the gain normalization term in the proposed FLL i.e. denominator of eq. (7d) is not the same as that of GI-FLL (2d) and GIO-FLL (4d). However, they are very similar and the difference appears from the definition of the state variables used in the both FLLs. To demonstrate this, let us consider the standard FLL given by eq. (2d) or (4d). By plugging the value of η_{ds} and η_{qs} in eq. (2d), the following can be obtained:

$$\dot{\hat{z}} = \frac{-\beta\hat{\omega}\eta_{qs}e}{\eta_{ds}^2 + \eta_{qs}^2} = \frac{\beta\hat{\omega}\cos(\hat{\theta})e}{\hat{A}} \tag{11}$$

Similarly, by plugging the values of η_1 and η_2 (given in eq. (6) in the proposed FLL (7d), the dynamics of the proposed FLL can be obtained as:

$$\begin{aligned}\dot{\hat{z}} &= \frac{-\beta_f\hat{\eta}_1\hat{\omega}e_f}{\hat{\eta}_1^2 + (\hat{\eta}_2/\hat{\omega})^2} \\ &= \frac{-\beta_f\left(\frac{1}{\omega_n^2+\hat{\omega}^2}\left\{-\frac{\hat{\omega}}{\omega_n}\hat{A}\cos(\hat{\theta}) + \hat{A}\sin(\hat{\theta})\right\}\right)\hat{\omega}e_f}{\frac{\hat{A}^2}{\omega_n^2(\omega_n^2+\hat{\omega}^2)}} \\ &= \frac{-\beta_f\omega_n^2\left\{-\frac{\hat{\omega}}{\omega_n}\cos(\hat{\theta}) + \sin(\hat{\theta})\right\}\hat{\omega}e_f}{\hat{A}}\end{aligned} \tag{12}$$

By comparing the standard FLL (11) and the proposed FLL (12) one can find that the denominator term is the same in both FLL. However, the numerator term is slightly different and the difference comes from the fact that the variables used in standard FLL and the proposed FLL are not the same by definition.

D. Stability analysis and tuning

To analyze the stability of the proposed filter, let us reconsider the filter as given in eq. (7a). By substituting $e_f = \nu - C_f\hat{\eta}$, eq. (7a) can be rewritten as

$$\dot{\hat{\eta}} = A_c\hat{\eta} + L_f\nu \tag{13}$$

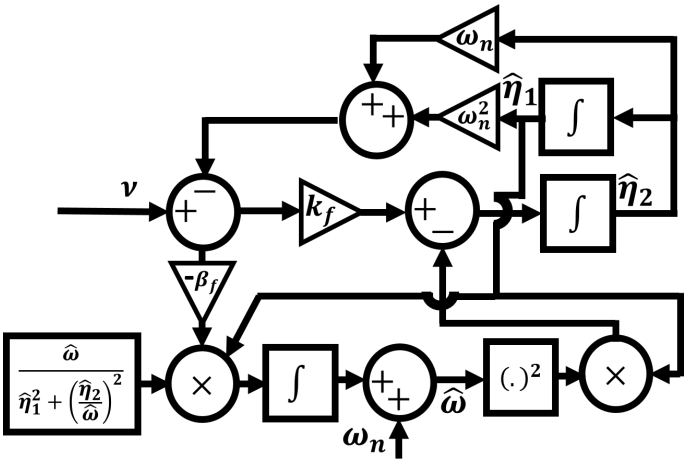

Figure 6. Block diagram of the GTF-FLL.

where

$$A_c = \hat{A}_f - L_f C_f = \begin{bmatrix} 0 & 1 \\ -(\hat{\omega}^2 + k_f\omega_n^2) & -k_f\omega_n \end{bmatrix}.$$

For essentially bounded and strictly positive estimated frequency $\hat{\omega}$, system matrix A_c is Hurwitz. Moreover, the input signal ν is sinusoidal. As such, the input signal is also essentially bounded. Then bounded input bounded output (BIBO) stability of the proposed filter can be easily shown by considering a quadratic Lypunov function similar to Theorem A2 in [39]. Once the BIBO stability of the filter is established, then boundedness of the signal estimation error and exponential decay of the estimation error can be established by using Theorem A3 in [39]. Since the results are straightforward to obtain, they are avoided here for the purpose of brevity. It is to be noted here that the adaptive filter presented in [39] is the same as the GI type adaptive observer presented in Sec. (II-B). As such, the results presented in [39] have the same frequency domain limitation as described in Sec. (II-B).

GTF-FLL has two parameters to tune, GTF gain k_f and the FLL gain β_f. To maintain complex conjugate poles with negative real parts, k_f should be selected inside the range $0 < k_f \leq 4.82$. For $k_f = 3$, GTF poles are located in $\omega_n(-1.5 \pm 1.32i)$. FLL gain β_f determines the convergence speed of the frequency estimation. Larger value of β_f results in faster convergence however at the cost of large overshoot and vice-versa. As such, β_f has to be selected as a trade-off between fast convergence and acceptable transient performance. Through extensive simulation, $\beta_f = 0.005$ has been found to give good results. This value can be considered as a good starting point.

To implement the proposed technique, Eq. (7) and (10) are required. Block diagram of the proposed frequency estimation approach is given in Fig. 6.

E. Extension to three-phase system

Single-phase GTF-FLL proposed in Section II-C can be easily applied to three-phase case. In general, the voltage vector of a three-phase unbalanced system is given by:

$$v_{abc} = \begin{bmatrix} v_a \\ v_b \\ v_c \end{bmatrix} = \begin{bmatrix} A_a \sin(\omega t + \phi_a) \\ A_b \sin(\omega t + \phi_b) \\ A_c \sin(\omega t + \phi_c) \end{bmatrix} \tag{14}$$

The voltage v_{abc} can be decomposed into $v_{abc} = v^+_{abc} + v^-_{abc} + v^0_{abc}$ where $+, -$ and 0 represents the positive, negative and zero sequences respectively and defined as:

$$v^+_k = A^+ \sin(\omega t + \phi^+ - k(120^0)) \tag{15a}$$
$$v^-_k = A^- \sin(\omega t + \phi^- + k(120^0)) \tag{15b}$$
$$v^0_k = A^0 \sin(\omega t + \varphi^0) \tag{15c}$$

where $k = a, b, c$ or $k = 0, 1, 2$ depending on the context. The sequences then can be calculated by the following relationships [40]:

$$v^+_{abc} = T_2 v_{abc} + T_1 v^{90^\circ}_{abc} \tag{16a}$$
$$v^-_{abc} = T_2 v_{abc} - T_1 v^{90^\circ}_{abc} \tag{16b}$$
$$v^0_{abc} = (I_3 - 2T_2) v_{abc} \tag{16c}$$

where $v^{90^\circ}_{abc}$is the 90° shifted signal, I_3 is the identity matrix of dimension 3×3 and

$$T_1 = \frac{\sqrt{3}}{6}\begin{bmatrix} 0 & 1 & -1 \\ -1 & 0 & 1 \\ 1 & -1 & 0 \end{bmatrix},$$
$$T_2 = \frac{1}{3}\begin{bmatrix} 1 & -0.5 & -0.5 \\ -0.5 & 1 & -0.5 \\ -0.5 & -0.5 & 1 \end{bmatrix}$$

Since GTF generates quadrature signal, it can be used to estimate the 90° shifted signal required in the sequence calculation given in Eq. (16a)-(16c).

III. Results and Discussions

A. Comparison with standard generalized integrator

In this Section, numerical simulation study will be provided to demonstrate the dynamic performance improvement by the proposed GTF. For this purpose, GTF and GI without FLL's are considered. The parameter of GI are selected as $k_s = \sqrt{2}$ and the GTF as $k_f = \sqrt{2}$ and 3. As explained in Sec. II-A, the tuning gain of standard GI always needs to satisfy $k_s < 2$ to main complex conjugate poles. For $k_f = k_s = \sqrt{2}$, both techniques have similar closed-loop pole locations. Comparative simulation results for the case of -0.5p.u.voltage sag is given in Fig. 7. Fig. 7 shows that when $k_f = k_s = \sqrt{2}$, both techniques have similar convergence time, however, the peak overshoot for GTF is smaller than GI. Moreover, when $k_f = 3$, GTF has significantly faster convergence time than that of GI.

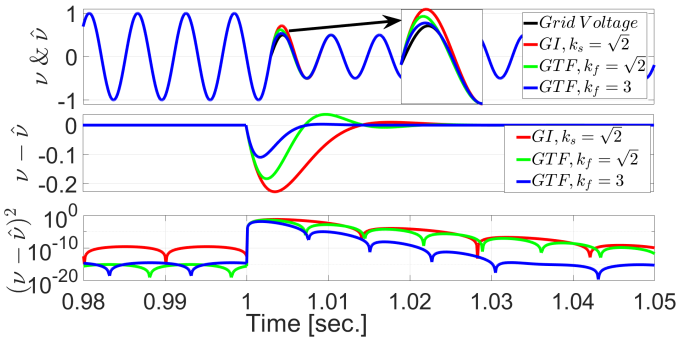

Figure 7. Comparative simulation results of GI and GTF for voltage sag case.

Table I
COMPARATIVE TIME DOMAIN PERFORMANCE SUMMARY.

	GTF-FLL	GI-FLL
$+2$Hz Frequency Change		
Settling time (± 0.1Hz.) (in cycles)	0.85	2.4
Settling time ($\pm 0.1^\circ$) (in cycles)	0.35	1.42
Peak frequency overshoot ($\lvert f - \hat{f} \rvert$)	0Hz	0Hz
Peak phase overshoot ($\lvert \theta - \hat{\theta} \rvert$)	2.4°	3.8°
-0.25p.u. Amplitude Change		
Settling time (± 0.1Hz.) (in cycles)	0.45	1.9
Settling time ($\pm 0.1^\circ$) (in cycles)	0.25	0.85
Peak frequency overshoot ($\lvert f - \hat{f} \rvert$)	1.3Hz	1Hz
Peak phase overshoot ($\lvert \theta - \hat{\theta} \rvert$)	3.9°	7.87°
$+45^\circ$ Phase Change		
Settling time (± 0.1Hz.) (in cycles)	1.62	3.45
Settling time ($\pm 0.1^\circ$) (in cycles)	1.7	4.25
Peak frequency overshoot ($f - \hat{f}$)	14.8Hz	5.2Hz
Peak phase overshoot ($\lvert \theta - \hat{\theta} \rvert$)	8.5°	9.7°

B. Experimental Results

This Section considers dSPACE 1104 board based experimental study. Overview of the experimental setup is given in Fig. 8. In the proposed experimental setup, dSPACE 1104 board is used to generate the grid voltage signal. dSPACE 1104 board has both digital-to-analog converter (DAC) output and analog-to-digital converter (ADC) input. So, the signal generated by the dSPACE 1104 board is first passed through the DAC block to get the physical analog signal. This analog signal is considered as the grid voltage signal and the whole process can be considered as the emulation of the grid voltage signal. This analog signal is then processed through the DAC input to feedback to the estimator algorithms implemented in dSPACE. So, the output of the DAC is physically connected to the ADC input. As such the proposed experimental study can be considered as hardware-in-the-loop (HIL) experimental one. HIL-type experimental study is widely considered in the grid synchronization literature [25], [41].

As comparison technique, we have selected the standard GI-FLL as described in Sec. II-A with the parameters as: $k_s = \sqrt{2}$ and $\beta_s = 50$. The parameters of GTF-FLL are selected as given in Sec. II-D. The considered sampling frequency is 10kHz. To test the proposed GTF-FLL, three challenging test scenarios are considered. They are:

- Test I: Sudden jump of $+2$Hz in frequency.
- Test II: Sudden jump of -0.25p.u. in amplitude.
- Test III: Sudden jump of $+45^\circ$ in phase.

Comparative experimental results are given in figures 9, 10, 11 for Test-I, II, and III respectively. Comparative experimental results demonstrate that the proposed GTF-FLL has very good convergence time w.r.t. GI-FLL. Comparative time domain performances are given in Table I.

From the settling time summary, it can be observed that the frequency estimation error for GTF-FLL converged $2.85, 4.22$, and 2.13 times faster than GI-FLL in Test-I, II, and III respectively. Similar excellent performances can be observed in the phase estimation error as well. These clearly demonstrates the dynamic performance improvement by the proposed GTF-FLL. Proposed GTF-FLL has higher peak overshoot for the frequency estimation in Test II and III. However, Test-III is unlikely to ever happen in actual power grid as this implies phase reversal. Moreover, in the control of grid-connected systems, synchronous reference frame (SRF) is widely accepted. In SRF, only the phase θ is required (*cf.* various control block diagrams presented in [42]). As such fast convergence of the phase estimation is more significant in control of grid-connected converters (GCC) than that of frequency estimation. In control theory, separation principles allows for separate tuning of estimator and controllers. Traditional approach to GCC control does include the dynamics of PLL/FLL in the controller parameter tuning and stability analysis. In this regard, if we can ensure that the phase estimation error converges really fast, then separation principle can be applied to GCC system as well from the practical viewpoint. This will allow separate tuning of controller leading to lower complexity in controller tuning. The proposed GTF-FLL can be considered as an important development in this context.

Tests I, II, and III do not consider any harmonics. However, low-order harmonics may not be avoided in some cases. To test the robustness of the proposed GTF-FLL, slightly distorted grid voltage signal with low-order harmonics are considered. In this case, the grid became suddenly polluted with low-order harmonics. The considered harmonics are: 3^{rd}- 1.9%, 5^{th} - 2.3%, 7^{th} - 1.7%, 9^{th} - 1.3%, and 11^{th} - 1.8%. Moreover, the grid frequency also changed from 50Hz to 52Hz. Experimental results for the harmonics robustness test are given in Fig. 12. From the experimental results in Fig. 12, it can be seen that both techniques have estimation ripples, which is normal in distorted grid. In this case, rise time can be a suitable performance metric than convergence time. By considering 90% of the final value as rise time threshold, the frequency rise time has been found to be ≈ 1 cycle for the proposed technique while it is ≈ 2 cycles for the standard GI-FLL. Similar excellent performance by the proposed GTF-FLL can be seen for the phase estimation error as well. Moreover, the ripples magnitude in the estimated phase is almost the same for both techniques.

As explained in Sec. II-E, proposed GTF-FLL can be easily extended to three-phase case. For this purpose, let us consider a balanced three-phase system i.e. $v^+_{abc} = 1\angle 0^\circ$. Suddenly due to fault, the system became unbalanced where the grid voltages became $v^+_{abc} = 0.65\angle -30^\circ$ and $v^-_{abc} = 0.35\angle 110^\circ$. Moreover, the frequency changed from 50Hz to 52Hz. Experimental

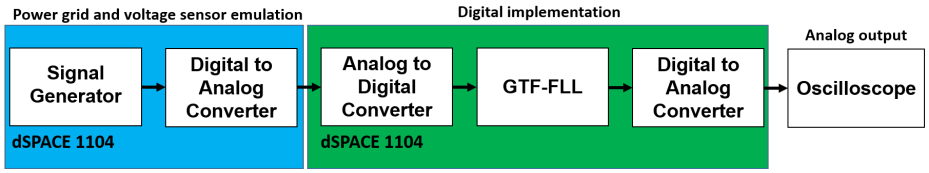

Figure 8. Block diagram of the experimental setup [25].

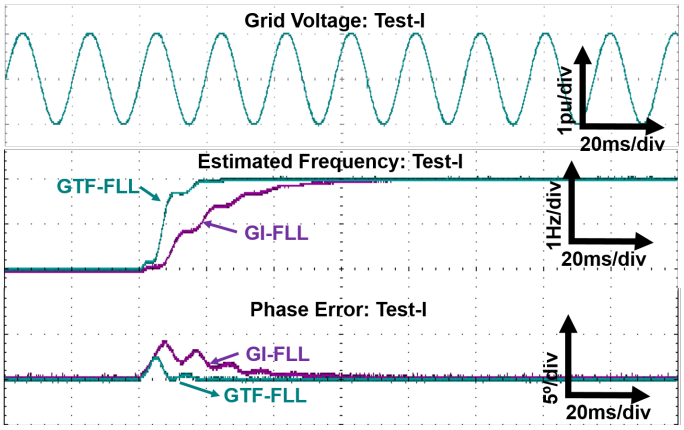

Figure 9. Comparative experimental results for Test I.

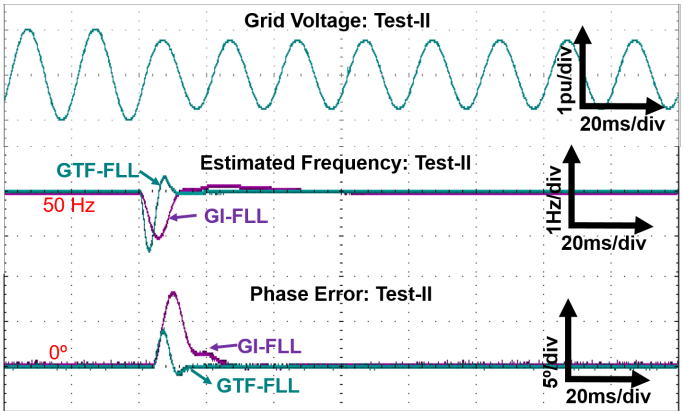

Figure 10. Comparative experimental results for Test II.

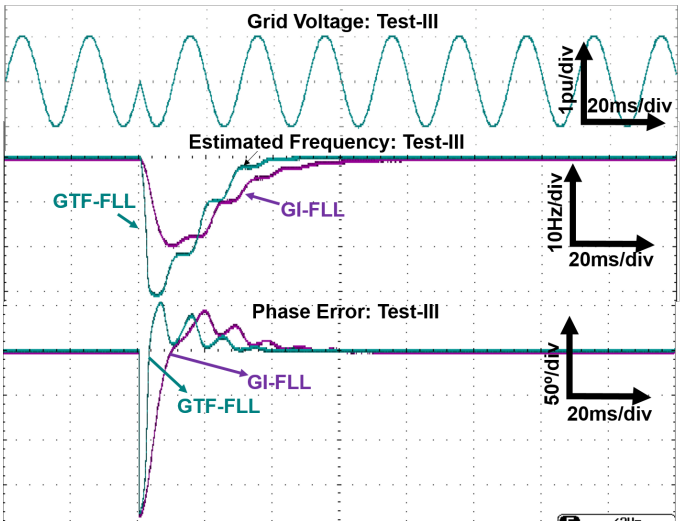

Figure 11. Comparative experimental results for Test III.

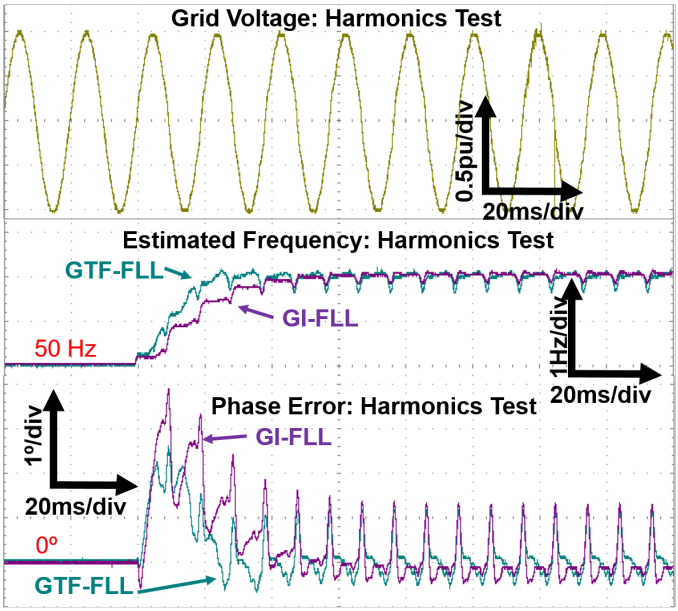

Figure 12. Experimental test results for harmonics polluted grid.

results in this case are given in Fig. 13. From Fig. 13, it can be seen that the proposed GTF-FLL successfully tracked the change in frequency with very fast convergence. Moreover, all the positive and negative sequence components are also successfully estimated very quickly as well. This demonstrates the suitability of the proposed technique for three-phase case.

IV. Conclusion

This paper demonstrated the application of a GI-type filter to estimate the parameters of grid voltage signals. The proposed technique uses a GI-QSG type dynamical model together with frequency-locked loop. The proposed filter uses coordinate transformation which helps to achieve an excellent trade-off between convergence speed and acceptable maximum peak estimation error. Comparative analysis have been performed

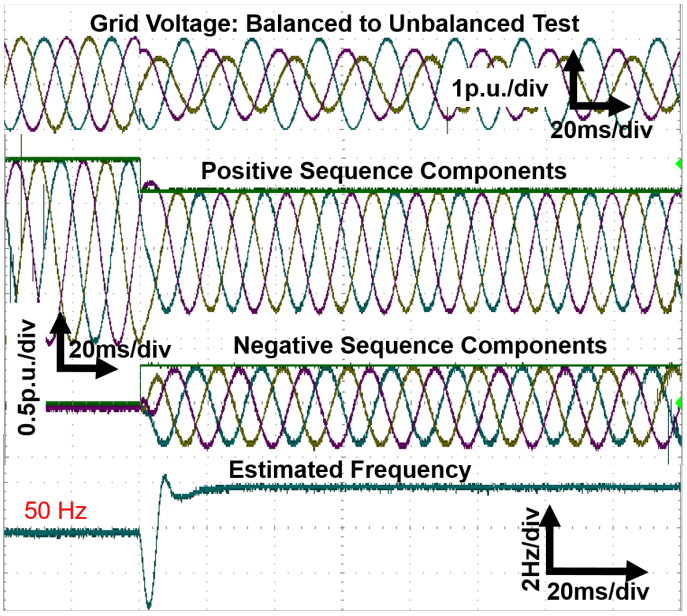

Figure 13. Experimental results for the three-phase case.

with GI-FLL using different challenging test scenarios. Test results demonstrated the suitability of the proposed approach.

ACKNOWLEDGMENT

We thank the anonymous reviewers for their critical reading of the manuscript.

REFERENCES

[1] G. Frigo, A. Derviškadić, Y. Zuo, and M. Paolone, "PMU-based ROCOF measurements: Uncertainty limits and metrological significance in power system applications," *IEEE Transactions on Instrumentation and Measurement*, vol. 68, no. 10, pp. 3810 – 3822, 2019.

[2] G. Frigo, A. Derviškadić, and M. Paolone, "Reduced leakage synchrophasor estimation: Hilbert transform plus interpolated DFT," *IEEE Transactions on Instrumentation and Measurement*, vol. 68, no. 10, pp. 3468 – 3483, 2018.

[3] K. Duda, T. P. Zieliński, A. Bień, and S. Barczentewicz, "Harmonic phasor estimation with flat-top FIR filter," *IEEE Transactions on Instrumentation and Measurement*, 2019.

[4] M. Merai, M. W. Naouar, I. Slama-Belkhodja, and E. Monmasson, "An adaptive PI controller design for DC-link voltage control of single-phase grid-connected converters," *IEEE Transactions on Industrial Electronics*, vol. 66, no. 8, pp. 6241–6249, 2018.

[5] A. Djoudi, S. Bacha, and H. Iman-Eini, "Efficient real-time estimation for DFIG-performance and reliability enhancement of grid/micro-grid connected energy conversion systems," *Journal of Renewable and Sustainable Energy*, vol. 11, no. 2, p. 025503, 2019.

[6] A. Boussaid, A. L. Nemmour, L. Louze, and A. Khezzar, "A novel strategy for shunt active filter control," *Electric Power Systems Research*, vol. 123, pp. 154–163, 2015.

[7] F. L. Yousfi, D. O. Abdeslam, T. Bouthiba, N.-K. Nguyen, and J. Merckle, "Adaline for online symmetrical components and phase-angles identification in transmission lines," *IEEE Transactions on Power Delivery*, vol. 27, no. 3, pp. 1134–1143, 2012.

[8] E. Jahan, M. R. Hazari, S. Muyeen, A. Umemura, R. Takahashi, and J. Tamura, "Primary frequency regulation of the hybrid power system by deloaded PMSG-based offshore wind farm using centralised droop controller," *The Journal of Engineering*, vol. 2019, no. 18, pp. 4950–4954, 2019.

[9] B. P. McGrath, D. G. Holmes, and J. J. H. Galloway, "Power converter line synchronization using a discrete fourier transform (DFT) based on a variable sample rate," *IEEE Transactions on Power Electronics*, vol. 20, no. 4, pp. 877–884, 2005.

[10] T. Tyagi and P. Sumathi, "Comprehensive performance evaluation of computationally efficient discrete Fourier transforms for frequency estimation," *IEEE Transactions on Instrumentation and Measurement*, pp. 1–1, 2019.

[11] Y. Amirat, Z. Oubrahim, G. Feld, and M. Benbouzid, "Phasor estimation for power quality monitoring: Least square versus Kalman filter," in *IECON 2017-43rd Annual Conference of the IEEE Industrial Electronics Society*. IEEE, 2017, pp. 4339–4343.

[12] Z. Oubrahim, V. Choqueuse, Y. Amirat, and M. E. H. Benbouzid, "Maximum-likelihood frequency and phasor estimations for electric power grid monitoring," *IEEE Transactions on Industrial Informatics*, vol. 14, no. 1, pp. 167–177, 2018.

[13] ——, "Disturbances classification based on a model order selection method for power quality monitoring," *IEEE Transactions on Industrial Electronics*, vol. 64, no. 12, pp. 9421–9432, 2017.

[14] R. Cardoso, R. F. De Camargo, H. Pinheiro, and H. Grundling, "Kalman filter based synchronisation methods," *IET generation, transmission & distribution*, vol. 2, no. 4, pp. 542–555, 2008.

[15] M. Qasim, P. Kanjiya, and V. Khadkikar, "Artificial-neural-network-based phase-locking scheme for active power filters," *IEEE Transactions on Industrial Electronics*, vol. 61, no. 8, pp. 3857–3866, 2014.

[16] H. Ahmed, S. Amamra, and I. Salgado, "Fast estimation of phase and frequency for single phase grid signal," *IEEE Transactions on Industrial Electronics*, vol. 66, no. 8, pp. 6408–6411, 2019.

[17] H. Ahmed, M. Bierhoff, and M. Benbouzid, "Multiple nonlinear harmonic oscillator-based frequency estimation for distorted grid voltage," *IEEE Transactions on Instrumentation and Measurement*, pp. 1–1, 2019.

[18] A. Kherbachi, A. Chouder, A. Bendib, K. Kara, and S. Barkat, "Enhanced structure of second-order generalized integrator frequency-locked loop suitable for DC-offset rejection in single-phase systems," *Electric Power Systems Research*, vol. 170, pp. 348–357, 2019.

[19] X. Yuan, W. Merk, H. Stemmler, and J. Allmeling, "Stationary-frame generalized integrators for current control of active power filters with zero steady-state error for current harmonics of concern under unbalanced and distorted operating conditions," *IEEE transactions on industry applications*, vol. 38, no. 2, pp. 523–532, 2002.

[20] C. M. Hackl and M. Landerer, "Modified second-order generalized integrators with modified frequency locked loop for fast harmonics estimation of distorted single-phase signals," *IEEE Transactions on Power Electronics*, vol. 35, no. 3, pp. 3298–3309, March 2020.

[21] F. Chishti, S. Murshid, and B. Singh, "Weak grid intertie WEGS with hybrid generalized integrator for power quality improvement," *IEEE Transactions on Industrial Electronics*, vol. 67, no. 2, pp. 1113 – 1123, 2020.

[22] H. Ahmed, S. Amamra, and M. H. Bierhoff, "Frequency-locked loop based estimation of single-phase grid voltage parameters," *IEEE Transactions on Industrial Electronics*, vol. 66, no. 11, pp. 8856–8859, 2019.

[23] M. L. Pay and H. Ahmed, "Modeling and tuning of circular limit cycle oscillator FLL with preloop filter," *IEEE Transactions on Industrial Electronics*, vol. 66, no. 12, pp. 9632–9635, 2019.

[24] A. Rahoui, A. Bechouche, H. Seddiki, and D. O. Abdeslam, "Grid voltages estimation for three-phase PWM rectifiers control without AC voltage sensors," *IEEE Transactions on Power Electronics*, vol. 33, no. 1, pp. 859–875, 2017.

[25] A. Safa, E. M. Berkouk, Y. Messlem, Z. Chedjara, and A. Gouichiche, "A pseudo open loop synchronization technique for heavily distorted grid voltage," *Electric Power Systems Research*, vol. 158, pp. 136–146, 2018.

[26] C. Subramanian and R. Kanagaraj, "Rapid tracking of grid variables using prefiltered synchronous reference frame PLL," *IEEE Transactions on Instrumentation and Measurement*, vol. 64, no. 7, pp. 1826–1836, 2014.

[27] H. Chaoui, O. Okoye, and M. Khayamy, "Grid synchronization phase-locked loop strategy for unbalance and harmonic distortion conditions," *Journal of Control, Automation and Electrical Systems*, vol. 27, no. 4, pp. 463–471, 2016.

[28] B. Lekouaghet, A. Boukabou, N. Lourci, and K. Bedrine, "Control of PV grid connected systems using MPC technique and different inverter configuration models," *Electric Power Systems Research*, vol. 154, pp. 287–298, 2018.

[29] C. Subramanian and R. Kanagaraj, "Single-phase grid voltage attributes tracking for the control of grid power converters," *IEEE Journal of Emerging and Selected Topics in Power Electronics*, vol. 2, no. 4, pp. 1041–1048, 2014.

[30] N. Jaalam, N. Rahim, A. Bakar, C. Tan, and A. M. Haidar, "A comprehensive review of synchronization methods for grid-connected

converters of renewable energy source," *Renewable and Sustainable Energy Reviews*, vol. 59, pp. 1471–1481, 2016.
[31] E. Radwan, K. Salih, E. Awada, and M. Nour, "Modified phase locked loop for grid connected single phase inverter," *International Journal of Electrical and Computer Engineering (IJECE)*, vol. 9, no. 5, pp. 3934–3943, 2019.
[32] V. Kaura and V. Blasko, "Operation of a phase locked loop system under distorted utility conditions," in *Proceedings of Applied Power Electronics Conference. APEC'96*, vol. 2. IEEE, 1996, pp. 703–708.
[33] M. Choukri Benhabib and S. Saadate, "A new robust experimentally validated phase locked loop for power electronic control," *EPE journal*, vol. 15, no. 3, pp. 36–48, 2005.
[34] A. Elrayyah, Y. Sozer, and M. Elbuluk, "Robust phase locked-loop algorithm for single-phase utility-interactive inverters," *IET Power Electronics*, vol. 7, no. 5, pp. 1064–1072, 2014.
[35] H. Ahmed and M. Benbouzid, "Simplified second-order generalized integrator-frequency-locked loop," *Advances in Electrical and Electronic Engineering*, vol. 17, no. 4, pp. 405–412, 2019.
[36] S. M. Shinners, *Advanced modern control system theory and design*. John Wiley & Sons, Inc., 1998.
[37] R. Teodorescu, M. Liserre, and P. Rodriguez, *Grid converters for photovoltaic and wind power systems*. John Wiley & Sons, 2011, vol. 29.
[38] H. Ahmed, M. Pay, M. Benbouzid, Y. amirat, and E. Elbouchikhi, "Hybrid estimator-based harmonic robust grid synchronization technique," *Electric Power Systems Research*, vol. 177, p. 106013, 2019.
[39] C. M. Hackl and M. Landerer, "A unified method for online detection of phase variables and symmetrical components of unbalanced three-phase systems with harmonic distortion," *Energies*, vol. 12, no. 17, p. 3243, 2019.
[40] D. Yazdani, A. Bakhshai, G. Joos, and M. Mojiri, "A real-time extraction of harmonic and reactive current in a nonlinear load for grid-connected converters," *IEEE Transactions on Industrial Electronics*, vol. 56, no. 6, pp. 2185–2189, 2009.
[41] S. Golestan, J. M. Guerrero, J. C. Vasquez, A. M. Abusorrah, and Y. Al-Turki, "Advanced single-phase DSC-based PLLs," *IEEE Transactions on Power Electronics*, vol. 34, no. 4, pp. 3226–3238, 2018.
[42] A. Micallef, "Review of the current challenges and methods to mitigate power quality issues in single-phase microgrids," *IET Generation, Transmission & Distribution*, vol. 13, no. 11, pp. 2044 – 2054, 2019.

Hafiz Ahmed (S'10--M'17) received the B.Sc. degree in Electrical & Electronic Engineering from Ahsanullah University of Science and Technology, Dhaka, Bangladesh, in 2011, the M.Sc. degree in Systems, Control and Information Technology from Joseph Fourier University, Grenoble, France, in 2013, and the Ph.D. degree in Automatic Control from the University of Lille 1, France, in 2016.
For the Ph.D. thesis, he received the EECI (European Embedded Control Institute) Ph.D. award, 2017. He is also the recipient of the Best PhD Theses award from the Research Cluster on Modeling, Analysis and Management of Dynamic Systems (GDR-MACS) of the National Council of Scientific Research (CNRS) in France in 2017. He was a Postdoctoral fellow at Clemson University, SC, USA followed by academic appointments in Bangladesh at the University of Asia Pacific and North South University. Since September 2017, he joined the School of Mechanical, Aerospace and Automotive Engineering, Coventry University, United Kingdom. He is interested in applied control engineering with special focus in energy and environment. He is an Associate Editor of the INTERNATIONAL JOURNAL OF ELECTRICAL ENGINEERING & EDUCATION.

Mohamed Benbouzid (S'92--M'95--SM'98--F'20) received the B.Sc. degree in electrical engineering from the University of Batna, Batna, Algeria, in 1990, the M.Sc. and Ph.D. degrees in electrical and computer engineering from the National Polytechnic Institute of Grenoble, Grenoble, France, in 1991 and 1994, respectively, and the Habilitation à Diriger des Recherches degree from the University of Picardie "Jules Verne," Amiens, France, in 2000.
After receiving the Ph.D. degree, he joined the Professional Institute of Amiens, University of Picardie "Jules Verne," where he was an Associate Professor of electrical and computer engineering. Since September 2004, he has been with the University of Brest, Brest, France, where he is a Full Professor of electrical engineering. Prof. Benbouzid is also a Distinguished Professor and a 1000 Talent Expert at the Shanghai Maritime University, Shanghai, China. His main research interests and experience include analysis, design, and control of electric machines, variable-speed drives for traction, propulsion, and renewable energy applications, and fault diagnosis of electric machines.
Prof. Benbouzid has been elevated as an IEEE Fellow for his contributions to diagnosis and fault-tolerant control of electric machines and drives. He is also a Fellow of the IET. He is the Editor-in-Chief of the INTERNATIONAL JOURNAL ON ENERGY CONVERSION and the APPLIED SCIENCES (MDPI) Section on Electrical, Electronics and Communications Engineering. He is a Subject Editor for the IET RENEWABLE POWER GENERATION. He is also an Associate Editor of the IEEE TRANSACTIONS ON ENERGY CONVERSION.